Optical high-order harmonic generation as a structural characterization tool

Lei Jia, Zhiya Zhang, D. Z. Yang, Yanqing Liu, M. S. Si, G. P. Zhang, and Y. S. Liu

Phys. Rev. B **101**, 144304 — Published 14 April 2020

DOI: 10.1103/PhysRevB.101.144304

Optical high-order harmonic generation as a structural characterization tool

Lei Jia, Zhiya Zhang, D. Z. Yang, Yanqing Liu, and M. S. Si*

Key Laboratory for Magnetism and Magnetic Materials of the Ministry of Education, Lanzhou University, Lanzhou 730000, China

G. P. Zhang†

Department of Physics, Indiana State University, Terre Haute, IN 47809, USA

Y. S. Liu

College of Physics and Electronic Engineering, Changshu Institute of Technology, Changshu 215500, China

(Dated: March 24, 2020)

Abstract

Structural characterization is essential to material engineering, but few tools can detect structural properties in time domain. High harmonic generation (HHG) emerges as a new frontier that touches the heart of condensed matter physics from the symmetry to quantum geometrical nature of electrons, but its capability in structural characterization has not been materialized. Here, we establish a crucial connection between the symmetry of a material and helicity of light. We employ monolayer MoS_2 as an example. We show that the linearly polarized laser pulse used in the experiments is not ideal for structural characterization because it only generates an in-plane anisotropy. It is the circularly polarized laser field that is capable of producing four distinctive HHG signals from the four phases of MoS_2. This finally links the laser helicity to the crystal structure. The results are generic and are not affected by the Berry curvature, the interband or intraband contribution. Our study unleashes the power of HHG as a structural characterization tool for technologically important materials.

I. INTRODUCTION

The high harmonic generation (HHG) has emerged as a promising tool to study the strong field effects and ultrafast electron dynamics in two-dimensional (2D) materials [1–3]. This inspires extensive investigations in 2D materials at attosecond timescale [3–8]. Recently, harmonic signals have been observed in graphene [9–11], MoS_2 [3, 12–15], and CrI_3 [16], where the harmonic signals crucially depend on the crystal symmetry. In graphene, only odd harmonics appear owing to the inversion symmetry [10, 11]. In contrast to graphene, even harmonics due to the broken inversion symmetry are observed in MoS_2 and CrI_3. The emerging even harmonics have attracted intense attention [3, 12, 13]. Liu and coauthors believed that the Berry curvature from the broken inversion symmetry gives rise to the even harmonics in MoS_2 [3]. However, their method ignores the effect of the interband polarization. Therefore, the correlation between the even harmonics and the Berry curvature in MoS_2 is still a matter of debate. It is also worth noting that some of symmetry properties of HHGs summarized in the Supplementary Information of Ref. [3] seem to be inconsistent with those in the main text. To this end, focus has been on the $1H$-semiconducting phase [3, 11–15, 17], but MoS_2 has another three common crystalline phases of $1T$, $1T^{'}$, and $1T_d$ [18]. The different phases have different electronic properties. For example, the $1T^{'}$ phase has a large quantum spin Hall effect while the $1T$ phase is metallic [19, 20]. The existence of these rich phases broadens the scope of monolayer MoS_2. However, since the $1T^{'}$ and $1T$ phases have similar crystal structures [20], how to distinguish them experimentally is extremely challenging. A similar phase transition is also found in $MoTe_2$ [7].

In this work, we demonstrate an unexplored capability of HHGs to distinguish crystalline phases of MoS_2 through laser helicity. The crystal symmetry has a remarkable impact on HHG signals. We find that when the laser is linearly polarized, even harmonics appear in $1H$- and $1T_d$-MoS_2 but disappear in $1T$- and $1T^{'}$-MoS_2. But the huge difference in HHG between two laser polarizations, parallel and perpendicular to the in-plane mirror symmetry, is unable to separate $1T$ from $1T^{'}$ phase. This shows the limitation of linearly polarized light [3]. We find that only circularly polarized light can do the job, where the four phases exhibit four remarkably different harmonics. $1H$-MoS_2 only has $3n \pm 1$ harmonics in-plane (n is an integer), $1T$-MoS_2 only has the $6n \pm 1$ in-plane harmonics and the $6n + 3$ out-of-plane harmonics, $1T^{'}$-MoS_2 only has odd harmonics, and the $1T_d$ phase has both even and

odd harmonics. These results show that the group symmetry difference leaves a distinctive hallmark on the harmonic signals that manifest themselves through laser helicity. This finding is expected to motivate further experimental investigations to develop HHG into a structure characterization tool at ultrafast time scale.

II. THEORETICAL METHOD

To fully appreciate the power of HHG, we choose MoS_2 which has four crystalline phases and has the quasi-two dimensional structure. We employ a generic Hamiltonian which reads

$$\mathscr{H} = \mathscr{H}_0 + \mathscr{H}_I(t), \tag{1}$$

where $\mathscr{H}_0$ is the ground state Hamiltonian that accounts for the electronic energy of solid and $\mathscr{H}_I(t)$ is the interaction Hamiltonian between the system and the femtosecond laser pulse. Before calculating the HHG, we self-consistently solve the Kohn-Sham equation [21], which is implemented in Wien2k [22]. Here, we ignore the crystal vibration induced by the irradiation of laser pulse. Once the calculation is converged, we construct the density matrix of ground state from $\rho_0 = |\Psi_{nk}\rangle\langle\Psi_{nk}|$, where Ψ_{nk} is the Bloch wavefunction of band n at crystal momentum k. We then obtain the dynamic density matrix by numerically solving the time-dependent Liouville equation $i\hbar\langle n\mathbf{k}|\partial\rho/\partial t|m\mathbf{k}\rangle = \langle n\mathbf{k}[\mathscr{H},\rho]m\mathbf{k}\rangle$ [23]. Finally, HHG is computed by Fourier transforming the induced macroscopic polarization $\mathbf{P}(t) = \sum_k \mathrm{Tr}[\rho_k(t)\hat{\mathbf{P}}_k]$ with $\hat{\mathbf{P}}_k$ being the momentum operator. $\mathscr{H}_I(t)$ is generally spatiotemporal and thus includes all the dynamical properties as well as symmetries. Whenever $\mathscr{H}_I(t)$ is invariant under a symmetry operation, the HHG must follow strict selection rules.

III. PROOF OF PRINCIPLES AND COMPARISON WITH EXPERIMENT UNDER LINEARLY POLARIZED LIGHT

Monolayer MoS_2 has four phases of $1H$, $1T$, $1T^{'}$, and $1T_d$. The most studied type is the $1H$ phase, but there has been no study of HHGs on the other three types. The $1H$ phase has a point group symmetry D_{3h} with an in-plane mirror symmetry (highlighted by the horizontal green line in Fig. 1(a)). We show below crystal symmetries manifest themselves in HHGs through the selection rules. When the laser field is linearly polarized along the x

axis, that is parallel to the mirror plane, only harmonics whose polarization is parallel to the field are generated from the $1H$-MoS_2, where both even and odd harmonics are present (see Fig. 1(a)). By contrast there is no signal perpendicular to the laser field. Since the wave propagation direction must be perpendicular to the electric field vector, harmonic signals can be spatially separated and detected by different cameras, as demonstrated in Fig. 1(a). This greatly eases the experimental detection.

However, when the laser field is polarized along the y axis (perpendicular to the mirror plane), the situation is entirely different. $1H$-MoS_2 emits harmonics along both the parallel and perpendicular directions (see Fig. 1(b)), with the parallel component being odd while the perpendicular one being even, fully consistent with the experimental results reported by Liu and coauthors [3]. But the Table 1 in the Supplementary Information contains an error in this configuration, where both even and odd harmonics are listed. The other three phases of MoS_2 yield slightly different HHGs with an in-plane anisotropy under linearly polarized laser (see the Supplemental Material [22]).

IV. HHG UNDER CIRCULARLY POLARIZED (σ) LIGHT

There has been no experimental investigation of HHG in MoS_2 under σ light, despite that the importance of light helicity has been recognized [3, 24]. In our study, when we use σ light within the xy plane, to our amazement, we find that four types of MoS_2 produce four distinctive harmonic signals. For instance, $1H$-MoS_2 presents signals with polarization parallel and perpendicular to the laser field, but has no out-of-plane signal along the z axis (see Fig. 2(a)). We also find that the harmonic orders are peculiar: only $3n-1$ and $3n+1$ order harmonics appear, while $3n$th order harmonics are missing, where n is an integer. However, this is no longer the case for $1T$-MoS_2. The harmonic orders of the in-plane polarization components are $6n+1$ and $6n-1$. The out-of-plane polarization component has an order of $6n+3$. For $1T'$-MoS_2, in contrast to the above two cases, the harmonic order in an arbitrary direction is odd (Fig. 2(c)). For $1T_d$-MoS_2, each polarization component contains both even and odd harmonics (Fig. 2(d)). Such different HHGs from the four phases of MoS_2 demonstrate that the HHGs from the circularly polarized light is capable of distinguishing different crystalline phases of monolayer MoS_2. Our finding now connects a pure theoretical result [6] with the structural characterization. In other words,

the experimental pattern of HHGs combined with the symmetries behind the selective rules would identify the phase of a material. This serves the basis of the HHG as a structure characterization tool.

V. PHYSICS BEHIND HHG OF MOS_2

The above findings are interesting, but the underlying mechanism has not been fully understood [6]. In $1H$-MoS_2, we see that the selective even harmonics only appear for a few particular polarization configurations. Moreover, the $3n$ order harmonics disappear for the in-plane polarization components when the laser field is circularly polarized. This means that some even harmonics are not protected by the Berry curvature under the σ light [3, 25].

Our dynamic density matrix ρ deduced from the Liouville equation indeed includes the complete information of the system (i.e., the interband and intraband transitions). More importantly, it also takes into account the crystal symmetry through $\mathscr{H}_I(t) = \sum_i O_i \hat{\mathbf{P}} \cdot \mathbf{A}(t)$, where O_i is the symmetry operation of a crystal, $\hat{\mathbf{P}}$ is the momentum operator, and $\mathbf{A}(t)$ is the vector potential of laser field. Importantly, we find that the symmetry operations O_i should be further classified into subgroups (SGs), depending on the laser polarization. In this way, the nth order of the time-dependent macroscopic polarization can be simplified as

$$P^{(n)}(t) = \gamma \sum_{SG} \sum_{i \in SG} O_i \hat{\mathbf{P}} \cdot \mathbf{A}^{(n)}(t), \tag{2}$$

where γ is the proportionality coefficient which has a complex expression [26, 27]. Commonly, O_i and $\hat{\mathbf{P}}$ cannot commute. Thus, the symmetry operation O_i can act on not only the momentum operator $\hat{\mathbf{P}}$ but also the laser vector field $\mathbf{A}(t)$.

In the following, we examine $1H$-MoS_2 under σ light excitation. The cases for the other three phases are presented in the Supplemental Material [22]. When the laser field is circularly polarized, the 12 symmetry operations of $1H$-MoS_2 should be classified into two subgroups SG_I and SG_{II}, as listed in Tab. SII of the Supplemental Material. Here, we take SG_I as an example. SG_I has six symmetry operations: E, C_3^1, C_3^2, σ_{xy}, $\widetilde{C_3^1}$, and $\widetilde{C_3^2}$. For in-plane σ light, no symmetry operation within SG_I changes the polarization direction of harmonics, and thus only one unit is formed [22, 28]. To ease the complexity of the calculation, we choose a single k point close to the Γ point to demonstrate the effect of the symmetry operations on HHG signals. Figure 3 shows the symmetry operation-resolved

harmonic signals. If we only employ the identity operation E, we will see that both even and odd harmonics appear both in-plane (Fig. 3(a)) and out-of-plane (Fig. 3(f)). This situation is the same when only the symmetry operations C_3^1 and C_3^2 are present (see the black lines in Figs. 3(b) and 3(g)).

However, when we sum over the signals generated under E, C_3^1 and C_3^2, only in-plane harmonics whose orders are $3n+1$ and $3n+2$ survive (Fig. 3(c)). This means that the symmetry adapted polarization cancels out the harmonics of other frequencies. Within the same SG_I, symmetry operations σ_{xy}, $\widetilde{C_3^1}$ and $\widetilde{C_3^2}$ have the same effect (Fig. 3(d)). Thus, when we sum over all the symmetry adapted polarizations, we only have $3n+1$ and $3n+2$ orders of harmonics (Fig. 3(e)). However, this exact summation cancels out the out-of-plane signal along the z axis (see Fig. 3(j)). It is also noticed that similar selection rules have been reported in molecules [29]. But the understanding of the underlying physics has not been given under the classification of the group symmetry.

We can understand the above finding analytically [30, 31]. The circularly polarized laser pulse has a vector potential as $\mathbf{A}(t) = A_0 \exp(-t^2/\tau^2)\cos(\varphi \pm \omega t)\hat{\mathbf{e}}_{xy}$, where A_0 is the amplitude, τ is the pulse duration, and $\varphi = \pi/4$ is the phase factor. For harmonic generation, the Gaussian pulse shape only changes the profile of the harmonic signal, and does not shift its frequency. For simplicity, we drop this term in the following analysis. Compared to the linearly polarized light, the phase factor φ provides an addition degree of freedom to modulate the selection rules of HHGs [22]. This dramatically changes the harmonic orders, which enables to distinguish the crystalline phases of MoS_2. The nth order electric polarization is proportional to the nth power of vector potential $\mathbf{A}(t)$. Following the same ideas in Eq. (2), we expand the polarization as

$$P_C^{(n)}(t) = \eta \sum_{SG} \sum_{i \in SG} O_i \hat{P} \frac{1}{2^n} \sum_{k=0}^{n} C_n^k \cos((2k-n)(\varphi \pm \omega t)), \tag{3}$$

where η is the reduced parameter. The in-plane polarization component of harmonics can be further clarified by introducing an operation as [31]

$$O_{xy}^C = (\varphi_i \to +2\pi/3, t \to +T/3)\,. \tag{4}$$

This operation of Eq. (4) requires the phase factor φ_i to be changed, which is absent for the linearly polarized laser field [22]. The change of one third of period both in the phase factor φ_i and the time t originates from the in-plane threefold rotational symmetry C_3^n. If

the crystal has another in-plane rotational symmetry, the order properties of HHGs will be changed accordingly [30].

Based on the operation in Eq. (4), the harmonic signals constrained from Eq. (3) appear if and only if

$$\cos((2k-n)(\varphi \pm \omega t)) = \cos((2k-n)(\varphi \pm \omega t) + (1 \pm (2k-n))2\pi/3). \tag{5}$$

Equation (4) dominates the selection rules of HHGs under the circularly polarized laser, giving rise to the $(3n \pm 1)$th order harmonics constrained by Eq. (5). Compared to the linearly polarized laser, the circularly polarized laser requires the selective vanishing of odd or even harmonics. This largely extends the application of HHG. All the above discoveries also hold for the other three phases: $1T$, $1T^{'}$, and $1T_d$ [22].

VI. ROLE OF BERRY CURVATURE

Liu and coauthors reported that the Berry curvature dominates the even harmonics [3], where only the intraband nonlinear current is taken into account. By contrast, in our calculations, we find that both the interband and intraband transitions contribute to the even harmonics due to the inversion symmetry breaking. Therefore, it seems necessary to reevaluate the influence of the Berry curvature on the even HHGs.

Among the four crystalline phases of MoS_2, the non-zero Berry curvature only appears in $1H$ or $1T_d$ structure [32]. Here, we take $1H$-MoS_2 to demonstrate the role of Berry curvature on the HHGs. According to the semiclassical theory, the role of the Berry curvature on the HHGs under the circularly polarized laser field can be evaluated by [32–34]

$$v(t) = \frac{\omega_B}{a} \sum_{n=1}^{\infty} \sum_{m=1}^{\infty} \Omega_n (-1)^m J_{2m-1}(\frac{n\omega_B}{\omega}) \left[\sin(2m(\varphi \pm \omega t)) - \sin((2m-2)(\varphi \pm \omega t))\right], \tag{6}$$

where Ω_n is the Fourier coefficient from expanding the Berry curvature, J_l is the Bessel function of the first kind of order l, a is the lattice constant of the crystal along the direction of the applied laser field, and $\omega_B = eE_0a/\hbar$ is the Bloch frequency. The inversion symmetry breaking enters the Berry curvature as it is expanded in sine Fourier series. According to the above analysis of the effect of crystal symmetry on the interband and intraband transitions, Eq. (6) should be invariant under the operation of the type: $\varphi_i \to +2\pi/3, t \to +T/3$. As a result, the Berry curvature gives rise to the $(6n \pm 2)$th order harmonics when the laser

field is circularly polarized, being covered in the above calculated HHGs. This result is very important and reveals that some even harmonics (i.e., the $6n$th order) would disappear under the circularly polarized laser field. In other words, the even harmonics are not necessarily protected by the Berry curvature. However, the intrinsic selection rule still works, which is rooted in the crystal symmetry [6]. In magnetically doped topological insulators, we also find that the broken inversion symmetry induces even harmonics, which stems from the effect of spin-orbit coupling [35]. In the meantime, we cannot exclude the appearance of even harmonics from the interband polarization as the electron transition immediately responds to the irradiation of laser pulse and then the intraband electronic dynamics occurs. In fact, the appearance of even harmonics from the Berry curvature is dominated by the inversion symmetry breaking regardless of the interband or intraband contribution.

VII. CONCLUSION

We have demonstrated that the HHGs from monolayer MoS_2 contain rich structural information about its crystalline symmetries and electronic properties. To understand the underlying physics, we classify the symmetry operations into several subgroups that preserve the laser polarization. The symmetry classification is different for the circularly and linearly polarized lasers. For example, in $1H$-MoS_2, we classify the 12 symmetry operations into three subgroups for the linearly polarized light. Each subgroup contains four symmetry operations (see Supplemental Material for more details). However, we can only classify the 12 symmetry operations into two subgroups for the circularly polarized light and each subgroup has 6 symmetry operations. This leads to different HHGs for the circularly and linearly polarized lasers. Our results suggest that the electronic property, the Berry curvature, the interband, and intraband transitions cannot alter the intrinsic selection rules of HHGs, which are instead dictated by the crystal symmetry. These findings demonstrate a novel feasible way to characterize the crystalline phases of MoS_2 through the emitted HHGs.

ACKNOWLEDGMENTS

We appreciate helpful communications with O. Neufeld. This work was supported by the National Science Foundation of China under Grant Nos. 11874189 and 11774139. We also

acknowledge the Fermi cluster at Lanzhou University for providing computational resources. GPZ was supported by the U.S. Department of Energy under Contract No. DE-FG02-06ER46304.

*sims@lzu.edu.cn

†guo-ping.zhang@outlook.com

[1] S. Ghimire and D. A. Reis, High-harmonic generation from solids, Nat. Phys. **15**, 10 (2019).

[2] Y. Yang, K. Lu, A. Manjavacas, T. S. Luk, H. Liu, K. Kelley, J.-P. Maria, E. L. Runnerstrom, M. B. Sinclair, S. Ghimire, and I. Brener, High-harmonic generation from an epsilon-near-zero material, Nat. Phys. **15**, 1022 (2019).

[3] H. Liu, Y. Li, Y. S. You, S. Ghimire, T. F. Heinz, and D. A. Reis, High-harmonic generation from an atomically thin semiconductor, Nat. Phys. **13**, 262 (2017).

[4] F. Krauzs and M. Ivanov, Attosecond physics, Rev. Mod. Phys. **81**, 163 (2009).

[5] P. B. Corkum and F. Krausz, Attosecond science, Nat. Phys. **3**, 381 (2007).

[6] O. Neufeld, D. Podolsky, and O. Cohen, Floquet group theory and its application to selection rules in harmonic generation, Nat. Commun. **10**, 405 (2019).

[7] J. Shi, Y.-Q. Bie, W. Chen, S. Fang, J. Han, Z. Cao, T. Taniguchi, K. Watanabe, V. Bulovic, E. Kaxiras, P. Jarillo-Herrero, K. A. Nelson, Terahertz-driven irreversible topological phase transition in two-dimensional $MoTe_2$, arXiv:1910.13609.

[8] E. J. Sie, C. M. Nyby, C. D. Pemmaraju, S. J. Park, X. Shen, J. Yang, M. C. Hoffmann, B. K. Ofori-Okai, R. Li, A. H. Reid, S. Weathersby, E. mannebach, N. Finney, D. Rhodes, D. Chenet, A. Antony, L. Balicas, J. Home, T. P. Devereaux, T. F Heinz, X. Wang, and A. M. Lindenberg, An ultrafast symmetry switch in a Weyl semimetal, Nature **565**, 61 (2019).

[9] I. Al-Naib, J. E. Sipe, and M. M. Dignam, High harmonic generation in undoped graphene: Interplay of inter- and intraband dynamics, Phys. Rev. B **90**, 245423 (2014).

[10] S.-Y. Hong, J. I. Dadap, N. Petrone, P.-C. Yeh, J. Hone, and R. M. Osgood, Jr., Optical third-harmonic generation in graphene, Phys. Rev. X **3**, 021014 (2013).

[11] N. Yoshikawa, T. Tamaya, and K. Tanaka, High-harmonic generation in graphene enhanced by elliptically polarized light excitation, Science **356**, 736 (2017).

[12] M.-X. Guan, C. Lian, S.-Q. Hu, H. Liu, S.-J. Zhang, J. Zhang, and S. Meng, Cooperative

evolution of intraband and interband excitations for high-harmonic generation in strained MoS_2, Phys. Rev. B **99**, 184306 (2019).

[13] T. Tamaya, S. Konabe, and S. Kawabata, Orientation dependence of high-harmonic generation in monolayer transition metal dichalcogenides, arxiv:1706.00548v1.

[14] N. Kumar, S. Najmaei, Q. Cui, F. Ceballos, P. M. Ajayan, J. Lou, and H. Zhao, Second harmonic microscopy of monolayer MoS_2, Phys. Rev. B **87**, 161403 (2013).

[15] L. M. Malard, T. V. Alencar, A. P. M. Barboza, K. F. Mak, and A. M. de Paula, Observation of intense second harmonic generation from MoS_2 atomic crystals, Phys. Rev. B **87**, 201401 (2013).

[16] Z. Sun,Y. Yi, T. Song, G. Clark, B. Huang, Y. Shan, S. Wu, D. Huang, C. Gao, Z. Chen, M. McGuire, T. Cao, D. Xiao, W.-T. Liu, W. Yao, X. Xu, and S. Wu, Giant nonreciprocal second-harmonic generation from antiferromagnetic bilayer CrI_3, Nature **572**. 497 (2019).

[17] K. F. Mak, C. Lee, J. Hone, J. Shan, and T. F. Heinz, Atomically thin MoS_2: A new direct-gap semiconductor, Phys. Rev. Lett. **105**, 136805 (2010).

[18] J. S. Sandoval, D. Yang, R. F. Frindt, and J. C. Irwin, Raman study and lattice dynamics of single molecular layers of MoS_2, Phys. Rev. B **44**, 3955 (1991).

[19] G. Eda, T. Fujita, H. Yamaguchi, D. Voiry, M. Chen, and M. Chhowalla, Coherent atomic and electronic heterostructures of single-layer MoS_2, ACS Nano **6**, 7311 (2012).

[20] X. Qian, J. Liu, L. Fu, and J. Li, Quantum spin Hall effect in two-dimensional transition metal dichalcogenides, Science **346**, 1344 (2014).

[21] G. P. Zhang, Y. H. Bai, and T. F. George, Energy- and crystal momentum-resolved study of laser-induced femtosecond magnetism, Phys. Rev. B **80**, 214415 (2009).

[22] For more detailed discussions and results of $1T$-, $1T^{'}$-, and $1T_d$-MoS_2, please see Supplemental Material at http://prb.aps.org/supplemental/, which also includes Refs. [36–41].

[23] G. P. Zhang, M. S. Si, M. Murakami, Y. H. Bai, and T. F. George, Generating high-order optical and spin harmonics from ferromagnetic monolayers, Nat. Commun. **9**, 3031 (2018).

[24] H. J. Simon and N. Bloembergen, Second-harmonic light generation in crystals with natural optical activity, Phys. Rev. **171**, 1104 (1968).

[25] S.-Y. Xu, Q. Ma, H. Shen, V. Fatemi, S. Wu, T.-R. Chang, G. Chang, A. M. M. Valdivia, C.-K. Chan, Q. D. Gibson, J. Zhou, Z. Liu, K. Watanabe, T. Taniguchi, H. Lin, R. J. Cava, L. Fu, N. Gedik, and P. Jarillo-Herrero, Electrically switchable Berry curvature dipole in the

monolayer topological insulator WTe_2, Nat. Phys. **14**, 900 (2018).

[26] C. L. Tang and H. Rabin, Selection rules for circularly polarized waves in nonlinear optics, Phys. Rev. B **3**, 4025 (1971).

[27] Y. Tokura and N. Nagaosa, Nonreciprocal responses from non-centrosymmetric quantum materials, Nat. Commun. **9**, 3740 (2018).

[28] G. P. Zhang and Y. H. Bai, Magic high-order harmonics from a quasi-one-dimensional hexagonal solid, Phys. Rev. B **99**, 094313 (2019).

[29] R. Baer, D. Neuhauser, P. R. Zdanska, and N. Moiseyev, Ionization and high-order harmonic generation in aligned benzene by a short intense circularly polarized laser pulse, Phys. Rev. A **68**, 043406 (2003).

[30] N. Saito, P. Xia, F. Lu, T. Kanai, J. Itatani, and N. Ishii, Observation of selection rules for circularly polarized fields in high-harmonic generation from crystalline solod, Optica **4**, 1333 (2017).

[31] O. E. Alon, V. Averbukh, and N. Moiseyev, Selection rules for the high harmonic generation spectra, Phys. Rev. Lett. **80**, 3743 (1998).

[32] D. Xiao, M. C. Chang, and Q. Niu, Berry phase effects on electronic properties, Rev. Mod. Phys. **82**, 1959 (2010).

[33] A. Chernikov, T. C. Berkelbach, H. M. Hill, A. Rigosi, Y. Li, O. B. Aslan, D. R. Reichman, M. S. Hybertsen, and T. F. Heinz, Exciton binding energy and nonhydrogenic Rydberg series in monolayer WS_2, Phys. Rev. Lett. **113**, 076802 (2014).

[34] T. T. Luu and H. J. Wörner, Measurement of the Berry curvature of solids using high-harmonic spectroscopy, Nat. Common. **9**, 916 (2018).

[35] Lei Jia, Zhiya Zhang, D. Z. Yang, M. S. Si, G. P. Zhang, and Y. S. Liu, High harmonic generation in magnetically-doped topological insulators, Phys. Rev. B **100**, 125144 (2019).

[36] J.-S. You, S. Fang, S.-Y. Xu, E. Kaxiras, T. Low, Berry curvature dipole current in the transition metal dichalcogenides family, Phys. Rev. B **98**, 12109(R) (2018).

[37] P. Blaha, K. Schwarz, P. Sorantin, and S. B. Trickey, Full-potential, linearized augmented plane wave programs for crystalline systems, Comput. Phys. Commun. **59**, 399 (1990).

[38] J. P. Perdew, K. Burke, and M. Ernzerhof, Generalized gradient approximation made simple, Phys. Rev. Lett. **77**, 3865 (1996).

[39] P. Blaha, K. Schwarz, G. K. H. Madsen, D. Kvasnicka, and J. Luitz, *WIEN2k, An Augmented*

Plane Wave + Local Orbitals Program for Calculating Crystal Properties (Karlheinz Schwarz, Techn. Universität Wien, Austria, 2001).

[40] D. Xiao, G.-B. Liu, W. Feng, X. Xu, and W. Yao, Coupled spin and valley physics in monolayers of MoS_2 and other group-VI dichalcogenides, Phys. Rev. Lett. **108**, 196802 (2012).

[41] R. Kappera, D. Voiry, S. E. Yalcin, W. Jen, M. Acerce, S. Torrel, B. Branch, S. Lei, W. Chen, S. Najmaei, J. Luo, P. M. Ajayan, G. Gupta, A. D. Mohite, and M. Chhowalla, Metallic 1T phase source/drain electrodes for field effect transistors from chemical vapor deposited MoS_2, APL Mater. **2**, 092516 (2014).

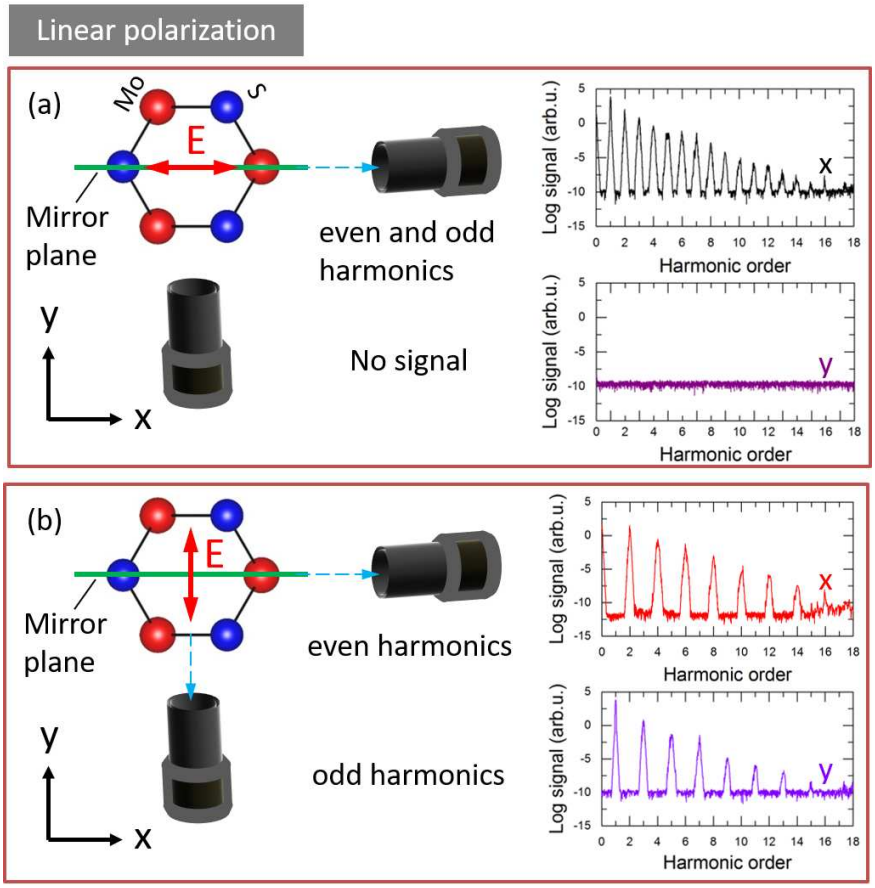

FIG. 1: High harmonic signals from $1H$-MoS_2 under two configurations: (a) parallel and (b) perpendicular. For the parallel configuration, the parallel polarization component has both even and odd harmonic signals. By contrast, for the perpendicular one, the cross harmonic signals are induced, where the even harmonics appear for the parallel component while the odd harmonics for the perpendicular component. The cameras are placed at the same plane of monolayer MoS_2. The dashed lines represent the emitted signals of HHGs. The parameters of laser field are taken as: A_0 = 0.03 Vfs/Å, $\hbar\omega$ = 1.0 eV, and τ = 60 fs.

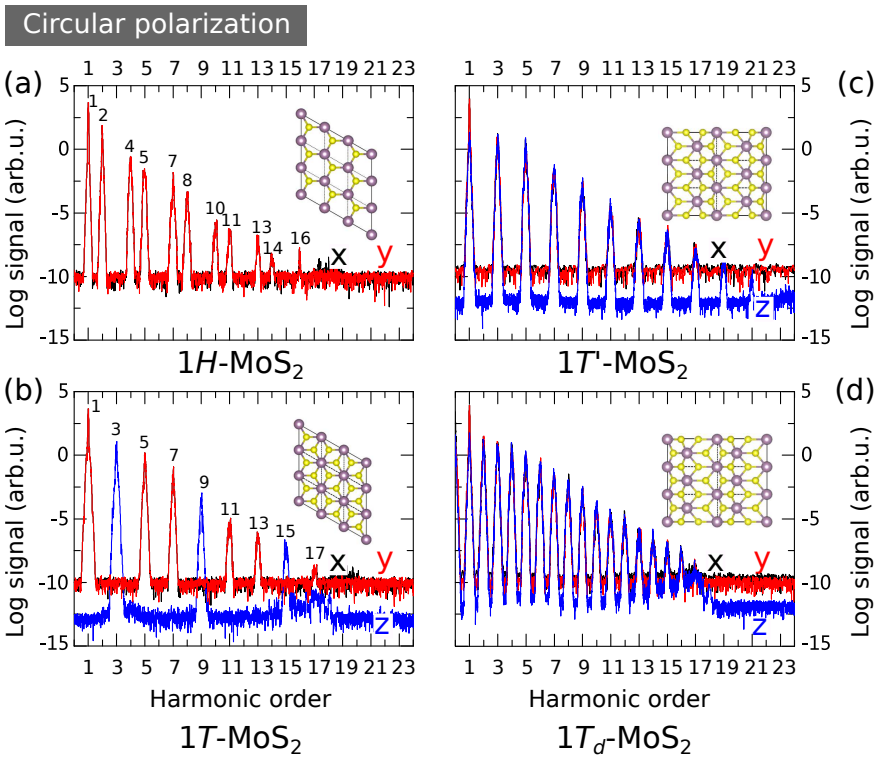

FIG. 2: High harmonic signals from MoS_2 when the laser field is circularly polarized. (a) The harmonic signals from $1H$-MoS_2, where the harmonic signals along the x and y axes appear while the harmonic signals along the z axis disappear. Interestingly, the harmonic order is $3n \pm 1$. (b) The harmonic signals from $1T$-MoS_2. In contrast to (a), the even harmonics disappear owing to the inversion symmetry and additional harmonics are induced along the z axis. (c) The harmonic signals from $1T^{'}$-MoS_2. Only odd harmonics appear. (d) The harmonic signals from $1T_d$-MoS_2. Even and odd harmonics coexist. All the parameters of laser pulse are the same as those in Fig. 1.

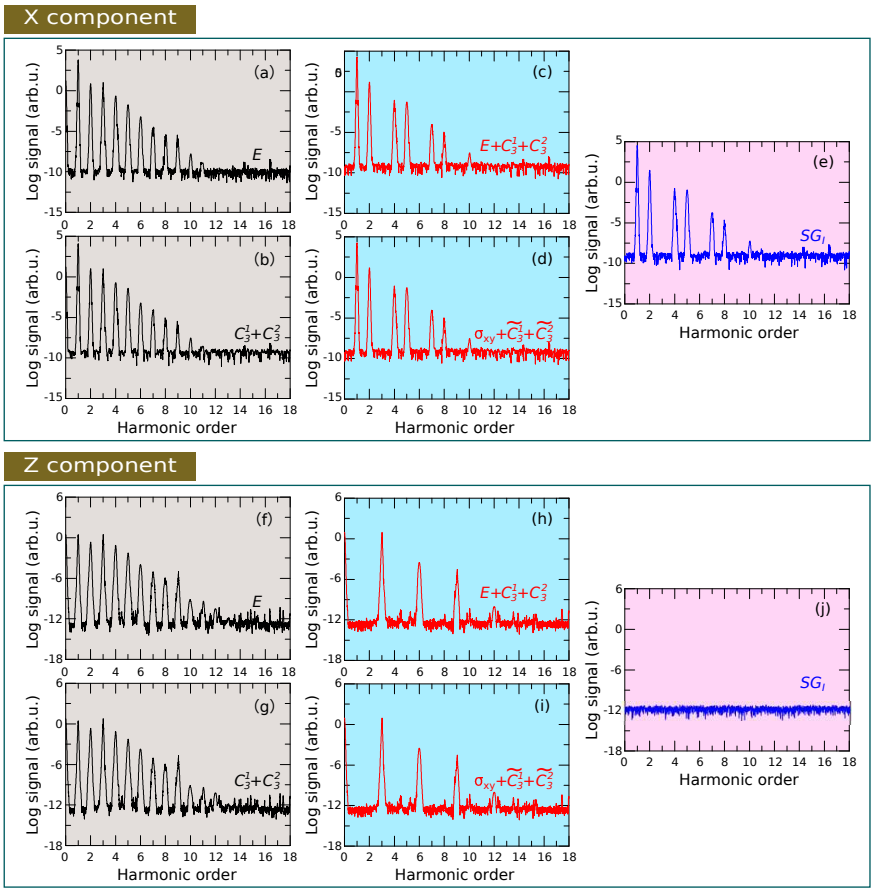

FIG. 3: Manifestation of group symmetry in HHG from $1H$-MoS_2 at the Γ point in the momentum space. Under the in-plane (xy) σ polarized light, the symmetry adapted HHG signals along the [(a)-(e)] x and [(f)-(j)] z axes have a distinctive dependence on symmetry operations. Date in (e) is the sum of (c) and (d) before Fourier transform. Date in (j) is the sum of (h) and (i), where the out-of-plane mirror reflection cancels out the harmonic signals. The parameters of laser pulse are the same as those in Fig. 1.